ARTICLE

Observed and Modelled Convective Mixing-Layer Height at Dome C, Antarctica

Giampietro Casasanta · Ilaria Pietroni · Igor Petenko · Stefania Argentini

Abstract The mixing-layer height is estimated using measurements from a high resolution surface-layer sodar run at the French-Italian station of Concordia at Dome C, Antarctica during the summer 2011–2012. The temporal and spatial resolution of the sodar allows the monitoring of the mixing-layer evolution during the whole diurnal cycle, i.e. a very shallow nocturnal boundary layer followed by a typical daytime growth. The behaviour of the summer mixing-layer height, variable between about 10- and 300 m, is analyzed as a function of the mean and turbulent structure of the boundary layer. Focusing on convective cases only, the retrieved values are compared with those calculated using a one-dimensional prognostic equation. The role of subsidence is examined and discussed. We show that the agreement between modelled and experimental values significantly increases if the subsidence is not kept fixed during the day. A simple diagnostic equation, which depends on the time-averaged integral of the near-surface turbulent heat flux, the background static stability and the buoyancy parameter, is proposed and evaluated. The diagnostic relation performance is comparable to that of the more sophisticated prognostic model.

Keywords Antarctica · Boundary layer · Mixing-layer height · Sodar

1 Introduction

The height of the atmospheric boundary layer (ABL) is an important variable, because it is commonly used in dispersion, climate, or numerical weather prediction models, and it is connected to the vertical extent of the turbulent exchange. With respect to environmental applications, the ABL height is often identified with the mixing-layer height (hereafter h).

G. Casasanta (✉) · I. Pietroni · I. Petenko · S. Argentini
Institute of Atmospheric Sciences and Climate, CNR, via del Fosso del Cavaliere 100, 00133 Rome, Italy
e-mail: g.casasanta@isac.cnr.it

I. Petenko
A.M. Obukhov Institute of Atmospheric Physics, RAS, Pyzhevskiy, 3, Moscow 119017, Russia

Despite its common use, a unique definition of h is not found in the literature, though after Cost action 710 an agreement seems to have been reached (Seibert et al. 2000) in considering h as "the height of the layer adjacent to the ground over which pollutants or any constituents emitted within this layer or entrained into it become mixed by convection or mechanical turbulence within a time scale of about one hour or less" (Beyrich 1997).

In Antarctica peculiar conditions occur: the continuous presence or absence of solar radiation during summer and winter, respectively. In addition, a different behaviour is observed in coastal and continental regions (King et al. 2006). The French-Italian permanent station of Concordia, over the Antarctic plateau at Dome C, provides the possibility of monitoring the evolution of the ABL during the whole year in one of the coldest places on Earth (Argentini et al. 2007). Despite the low air temperatures and sensible heat flux values at Dome C (Georgiadis et al. 2002), the ABL during the summer has a diurnal evolution similar to that observed at mid-latitudes (Mastrantonio et al. 1999; Van As et al. 2005; King et al. 2006). During the warmer hours of the day the upward sensible heat flux drives the formation of the convective mixing layer, characterized by h values up to about 400 m. In contrast, a shallow stable layer is often observed during the rest of the day (Argentini et al. 2005; Pietroni et al. 2012). The summer evolution of the ABL in Antarctica using sodars was widely investigated in previous works (e.g. Argentini et al. 2005, 2007; Neff et al. 2008). Pietroni et al. (2012) compared the mixing-layer height derived at Dome C by sodar measurements with estimations of the prognostic zero-order mixing-layer model of Gryning and Batchvarova (1990), hereafter GBmodel. The model performs well in the first part of the day, when the mixing layer is shallow, the sensible heat flux shows a monotonic behaviour, and the subsidence can generally be neglected. Some problems occur when the mixing layer deepens and the subsidence velocity may be comparable to the rate at which the mixed layer entrains into the air aloft (Batchvarova and Gryning 1994).

The mixing-layer height can also be determined using diagnostic models, based on the similarity theory, which represent approximated quasi-equilibrium relationships between relevant parameters (e.g. Zilitinkevich 1972; San Jose and Casanova 1988; Joffre and Kangas 2001; Joffre et al. 2001). Although these relations are applicable only under certain conditions (Seibert et al. 2000), they can be used in applications for which more sophisticated measurements are not available.

As the accuracy and the vertical resolution of the previous sodar measurements were not sufficient to resolve the fine structure of the mixing-layer behaviour, an improved acoustic remote sensing device (Mastrantonio et al. 2010; Argentini et al. 2012a), the Surface-Layer Mini-Sodar (hereafter SLM-Sodar) was specifically developed. The instrument was used for the first time during a field experiment carried out at Concordia station (Dome C, East Antarctica) during 2011–2012. In spite of the good performance of the SLM-Sodar (Argentini et al. 2013a), these measurements cannot be performed continuously on a routine basis due to the severe environmental conditions and the large effort needed to retrieve values of h from sodar profiles. The improvement of simple and well-tested parametrizations, based on standard surface or turbulent parameters observations, is a possible way to overcome this difficulty.

In this work, the SLM-Sodar measurements are used to test and develop parametrizations for the convective mixing-layer height estimation in polar regions. The paper is organized as follows: Sect. 2 describes the site, the instrumentation and the methodology used to derive h from high temporal and spatial resolution sodar measurements. Section 3 presents h as a function of heat and momentum fluxes. In Sect. 4, the role of subsidence in the GBmodel is studied, and a simple diagnostic relation is proposed and verified. Conclusions are given in Sect. 5.

2 Site, Instrumentations and Methods

The French-Italian station of Concordia is located at Dome C (74°06′S, 123°20′E), on the East Antarctic plateau, at 3,233 m a.s.l. In the framework of the Atmospheric Boundary Layer Climate (ABLCLIMAT) project, an experimental campaign was conducted between December 2011 and December 2012. The project focuses on the characterization of the ABL through acoustic remote sensing observations, and on the verification of boundary-layer parametrizations to be used in numerical meteorological models for polar regions.

During the experimental campaign the SLM-Sodar and a sonic anemometer on a mast were placed 400 m south-west of the base, upwind to the prevailing wind direction to avoid disturbances in measurements. Radio-soundings were carried out once a day, in the framework of the Routine Meteorological Observation program (RMO, www.climantartide.it). The sonic anemometer by Metek was operated at a sample frequency of 10 Hz, and after a quality check (Vickers and Mahrt 1997), the raw data were analyzed using the eddy-covariance technique (Lee et al. 2004; Aubinet et al. 2012) in order to derive the turbulent fluxes over a period of 10 min, performing despike, two-rotation and the cross-wind corrections.

The SLM-sodar performances are discussed in Argentini et al. (2012a), while specifications and system configurations used at Concordia during the 2012 field experiment are reported in Argentini et al. (2012b). During the summer period the carrier frequency was 2,000 Hz, the pulse duration 50 ms, and the pulse repetition rate 3 s, so that the maximum potential range was 360 m, with a lowest observation height and a vertical resolution of about 8 m.

Sodar measurements are based on the interaction of acoustic waves with atmospheric turbulence. Since the acoustic waves are scattered by small-scale temperature fluctuations, h can be estimated using objective or subjective methods applied to the digitalized range-corrected vertical profiles of the backscattered signal intensity (range corrected signal, hereafter RCS). In this work, the technique originally proposed by Beyrich (1993) and Beyrich and Weill (1993) was applied to the noise-corrected RCS. Under convective conditions (Fig. 1a), h was determined as the height above the zone of weak signal intensity (characterizing a well-mixed layer) at which an elevated maximum occurs, i.e. in correspondence with the zone of strong turbulence at the capping inversion base. Under stable conditions (Fig. 1b), h was retrieved either from the minimum of the first derivative, or from the maximum curvature of the RCS
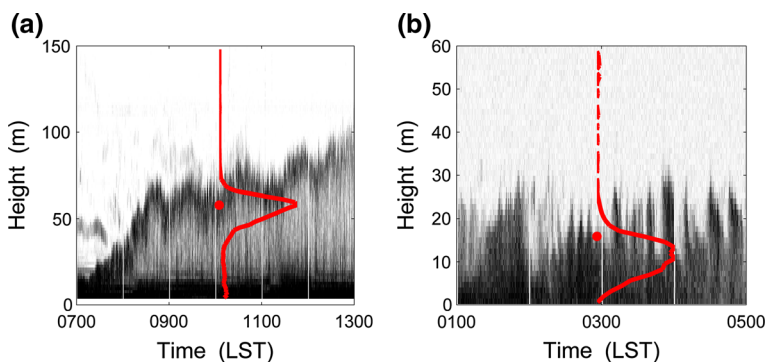
Fig. 1 Examples of sodargrams under convective (**a**, 12 December 2011) and stable (**b**, 5 February 2012) conditions. *Continuous lines* and *dots* represent the normalized range corrected signals and the estimated mixing-layer heights at 1005 and 0255 LST, respectively

Table 1 Scheme for h estimation based on sodar range-corrected profiles

ABL regime	Shape of the RCS	Applied method
Stable ABL	Continuous decrease with height	Maximum RCS curvature
	Non-monotonous decrease	RCS first derivative minimum
Convective ABL	Elevated maximum in RCS	Height of the maximum

profile, depending on the stage of ABL evolution and on the shape of the RCS profile (Beyrich et al. 1996; Beyrich 1997). The procedures used in both convective and stable conditions are summarized in Table 1.

During the period 11 December 2011–5 February 2012, a total of 37 days with high quality simultaneous sonic anemometer and SLM-Sodar measurements is available. Only 12 days of measurements related to clear-sky conditions and moderate near-surface wind speeds (<5 m s^{-1}) are considered herein. The turbulent kinematic heat flux at the surface, hereafter $\overline{(w'\theta')}_\mathrm{s}$, was used to select the cases with clear convective activity, $\overline{(w'\theta')}_\mathrm{s} > 0.004$ K m s^{-1}.

3 Mixing-Layer Evolution and Characterization

To characterize the development and the evolution of the mixing layer a statistical analysis was performed. As is the case at mid-latitudes, the mixing-layer behaviour at Dome C shows a daily cycle (Mastrantonio et al. 1999; Argentini et al. 2007), and despite the low surface sensible heat flux a mixing layer develops during the central part of the day (Georgiadis et al. 2002). Under these conditions, in a few cases the mixing-layer height surpasses 400 m (Argentini et al. 2005), depending on the sun's elevation and on the meteorological conditions. Figure 2 shows the 24-h distribution of the measured h, where the intensity of the grey scale gives the occurrence of a certain h value at each hour. The mixing layer is found in the first 50 m during the night, with a median value of 25 m; from 0600 local standard time (hereafter LST) a convective mixing layer develops and h increases gradually until about 1300 LST, when the maximum is reached and maintained for the following 2 h. Between 1000 and 1600 LST the h values are more dispersed than those observed in stable conditions, and the maximum ranges between 75 and 250 m with a median of 125 m. Around 1600 LST the
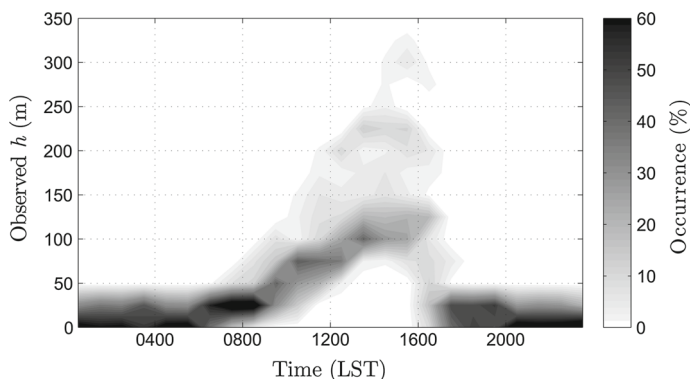
Fig. 2 24-h distribution of h estimated by SLM-sodar measurements (12 selected days in the period 11 December 2011–5 February 2012). The intensity of the *grey scale* gives the occurrence of a certain h value at each hour
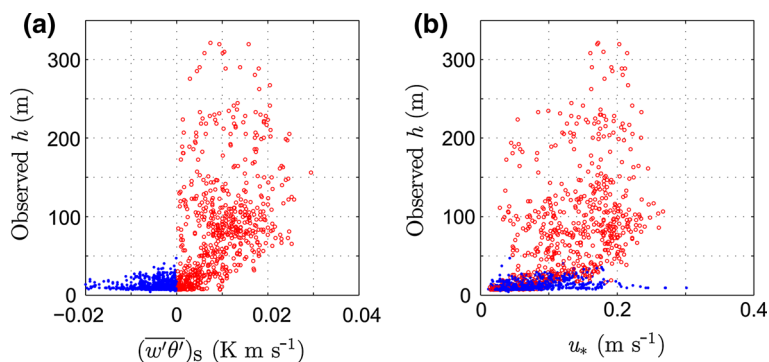
Fig. 3 Scatter plots of h determined from SLM-Sodar measurements and the micrometeorological parameters $(\overline{w'\theta'})_{\mathrm{s}}$ (**a**), and u_* (**b**) in both convective (*open red dots*) and stable cases (*blue dots*)

convective mixing layer collapses, and a stable layer forms near the ground. The presented results are similar to those obtained by Georgiadis et al. (2002), who for the period between 20 January and 3 February 1999 reported an average maximum value of 150 m. The h values reported in the literature for the entire summer (Argentini et al. 2005) are generally higher than those reported here, as the data screening considerably reduced the initial dataset, and half of the analyzed days refer to the period after 20 January, when the sun's elevation is low.

The micrometeorological parameters present the typical diurnal behaviour (King et al. 2006), characterized by increasing air temperature and wind speed during the central part of the day. The maximum of $(\overline{w'\theta'})_{\mathrm{s}}$ corresponds to the maximum of solar irradiance, as shown by Argentini et al. (2005). In the same paper it is also shown that the friction velocity (hereafter u_*) has a daily cycle with a plateau value, reached around midday and lasting 4 h. Figure 3 shows the dependences of h on $(\overline{w'\theta'})_{\mathrm{s}}$ (panel a) and u_* (panel b), in both unstable and stable cases. The values of both the variables are in agreement with those observed during the summer by Argentini et al. (2005), Georgiadis et al. (2002), and Mastrantonio et al. (1999). The scatter of the points in Fig. 3a is due to the different daily behaviour of $(\overline{w'\theta'})_{\mathrm{s}}$ and h; while the turbulent heat flux shows a maximum around midday, followed by a decreasing trend in the afternoon, the mixing layer reaches its maximum height approximately in the same period, but maintains this value at least for 2 h. An analogous scatter is shown in the u_* values under convective conditions (Fig. 3b), i.e. when mechanical turbulence is negligible and the mixing layer is convectively driven (Stull 1988).

4 Parametrizations

Simple diagnostic and prognostic parametrizations to estimate h are very attractive, because generally require a few input parameters, and can be adopted for operational use. In Sect. 4.1 the performance of the prognostic Gryning–Batchvarova (GB) model to estimate h under unstable conditions is evaluated, and the role of the subsidence is investigated. In Sect. 4.2 a simple diagnostic model is proposed and tested.

4.1 Gryning–Batchvarova Model

As proposed by Batchvarova and Gryning (1994) the evolution of the mixing-layer height is given by the following expression,
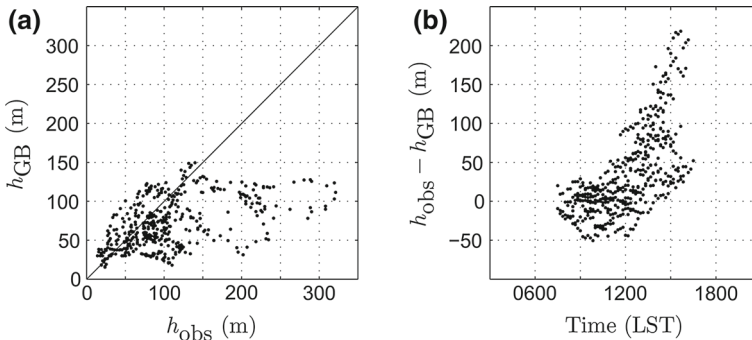
Fig. 4 **a** Scatter plot of *h values* derived by the SLM-Sodar and GBmodel (with $w_s = 0.04$ m s^{-1}); the *full line* represents the 1:1 line. **b** Difference between measured and computed *h* as a function of the time

$$\left\{ \left(\frac{h^2}{(1+2A)\,h - 2BkL} \right) + \frac{Cu_*^2 T}{\gamma g \left[(1+A)\,h - BkL \right]} \right\} \left(\frac{dh}{dt} - w_s \right) = \frac{\left(\overline{w'\theta'} \right)_s}{\gamma}, \quad (1)$$

where k is the von Karman constant ($k = 0.4$), g is the acceleration due to gravity, γ is the potential temperature gradient in the free atmosphere, w_s is the mean vertical motion at the mixing-layer top (the so-called subsidence velocity is by definition the negative of w_s), L and T are the Obukhov length and the near-surface temperature, respectively, and A, B, C are empirical constants set to 0.2, 2.5 and 8 (Batchvarova and Gryning 1990, 1994). In Eq. 1 the mechanical and thermal turbulence are represented by the first term on the left-hand side, while the spin-up effect is the second term. The spin-up effect is important in the morning, i.e. when the mixing layer is shallow. Equation 1 was solved numerically for periods in which the kinematic heat flux was always positive, fixing the initial $h = 30$ m. For each day, the value of γ was determined using the radiosounding temperature profile at about 2000 LST, and kept fixed throughout the day. The γ values ranged between 0.001 and 0.015 K m^{-1}. To evaluate the uncertainty introduced by using a fixed γ value, its diurnal behaviour was investigated by radiosounding profiles acquired at other coastal and plateau (McMurdo and Amundsen-Scott) stations. The retrieved uncertainty on h was <10 %. Following Pietroni et al. (2012), the value of w_s was initially fixed to -0.04 m s^{-1}. Figure 4a shows the scatter plot between h estimated by the SLM-Sodar and those given by the GBmodel. The index of agreement (*IoA*) = 0.57, while the root-mean-square error (*rmse*) = 69 m. These values are comparable with those found by Pietroni et al. (2012). Figure 4b shows the difference between the experimental and the modelled value of h during the day; as shown in Pietroni et al. (2012), the model performs well in the first part of the day. The major discrepancies are found in the second part of the day, i.e. when $(\overline{w'\theta'})_s$ shows a typical decreasing trend (Georgiadis et al. 2002; King et al. 2006), while the other external parameters are kept fixed.

As shown by Batchvarova and Gryning (1994), the diurnal evolution of w_s is relevant and should be considered. To investigate the dependence of h on w_s, a simple relationship between this parameter and time was derived. The dataset was divided into two subsets with the values of h and turbulent fluxes varying in the same ranges. The values of w_s were then computed applying the GBmodel to one of the subset, using the h values observed by sodar. Figure 5 shows the scatterplot of w_s with time t, the latter expressed in seconds since midnight. A linear regression (continuous straight line) was used to parametrize w_s as $w_s = at + b$, where $a = (1.43 \pm 0.37)10^{-6}$ m s^{-2} and $b = (-0.097 \pm 0.017)$ m s^{-1}. This relationship was then used to retrieve the w_s-dependent h values from the second dataset. The comparison

Fig. 5 Dependence of w_s on the hour of the day. The *black line* represents the linear fit with the expression $w_s = 1.43 \times 10^{-6}t - 0.097$, where time t is expressed in seconds since midnight
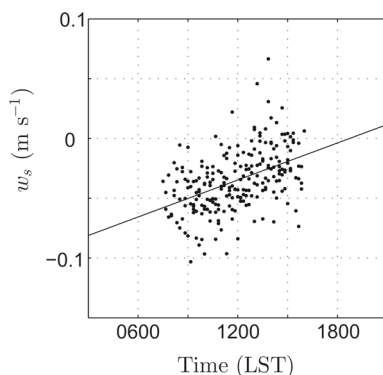
Fig. 6 Scatter plot of h derived by SLM-Sodar and GBmodel with w_s fix during the day (*black dots*) and w_s variable and obtained from Eq. 2 (*green stars*). The *full line* represents the 1:1 line
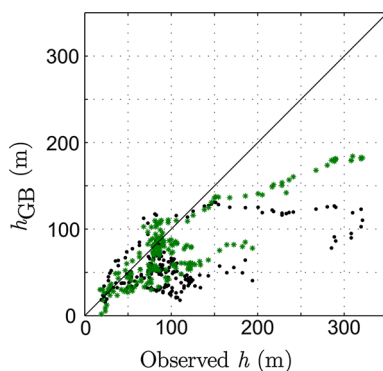
Table 2 Performance of the GBmodel with fixed (second column) and variable (third column) value of w_s, of the encroachment model (EM) (fourth column), and of the diagnostic relation (fifth column)

Parameter	Fixed w_s	Variable w_s	EM	Diagnostic relation
mae (m)	41	33	79	29
rmse (m)	69	49	92	42
FB	0.53	0.29	−0.53	0.19
IoA	0.57	0.84	0.72	0.84

The listed parameters (first column) are the mean absolute error (*mae*), the root-mean-square error (*rmse*), the fractional bias (*FB*, varying between −2 and 2), and the index of agreement (*IoA*)

between h estimated by the SLM-Sodar measurements and the GBmodel with fixed (black dots) and variable (grey stars) w_s values is shown in Fig. 6. Table 2 gives some relevant statistical parameters that summarize the model performance: the mean absolute error (*mae*), the *rmse*, the fractional bias (*FB*, varying between −2 and 2) and the *IoA*. A model has a good performance when the *IoA* value is close to unity, and *mae*, *rmse* and *FB* close to zero. The introduction of a variable w_s leads to more accurate predictions, although the GBmodel still tends to slightly underestimate h (*FB* = 0.29). By way of example, Fig. 7 shows the prediction of the GBmodel with fixed (green full line) and variable (blue full line) w_s for an entire day (3 January 2012).

Figure 5 shows a general picture of descending motion, with the subsidence decreasing from the morning to the afternoon. This trend is different from what would be expected—i.e.
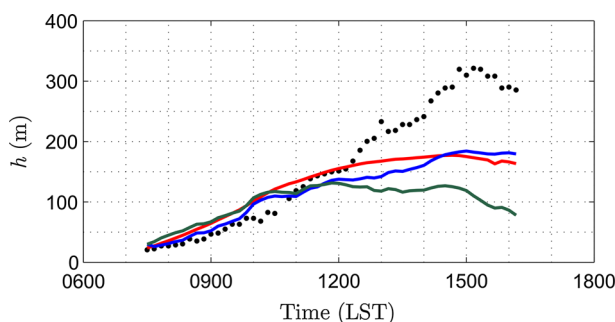
Fig. 7 Mixing-layer heights computed with Eq. 4 (*red full line*), and the GB model with fix (*green full line*) and variable (*blue full line*) w_s values for 3 January 2012. *Dots* represent the experimental h data estimated from sodar measurements

an increase in the subsidence when the mixing-layer height increases (see, e.g., Ouwersloot et al. 2012)—using the hypothesis of a horizontal divergence constant with height. The anomalous behaviour observed at Concordia is due to the presence of gravity flows (Argentini et al. 2013b, which are more intense in the morning than during the warmer hours of the day. The decrease in the gravity flow intensity implies smaller values of the horizontal divergence, and consequently of the subsidence. This phenomenon is somehow similar to that observed at mid-latitudes by others (see, e.g., Myrup et al. 1983; Kossmann et al. 1998; Faloona et al. 2013) in the presence of mesoscale systems (upslope flows, valley winds, and sea breezes).

Equation 1 requires knowledge of a certain number of parameters, some of them provided by measurements that are not routinely available. To overcome this issue, when the mechanical turbulence is weak the simple encroachment model,

$$\frac{\mathrm{d}h}{\mathrm{d}t} = \frac{\left(\overline{w'\theta'}\right)_s}{h\gamma}, \tag{2}$$

is often used. For operational use, the encroachment model is considered a simple way to calculate h, and it is known to perform well under convective conditions (Batchvarova and Gryning 1990). Equation 2 was solved numerically for the same dataset used to test the w_s-dependent GBmodel, fixing the initial $h = 30$ m. Its performance is summarized in Table 2. Despite the good agreement ($IoA = 0.72$), the encroachment model tends to overestimate h ($FB = -0.53$), and both the *mae* and the *rmse* values are appreciably higher than those related to the GBmodel. In order to retrieve an equally simple relation to model the mixing-layer behaviour under the peculiar conditions at Dome C, as described in the next section a diagnostic equation was developed and evaluated.

4.2 A Simple Diagnostic Relation

Despite the convective mixing-layer height being generally treated in terms of prognostic equations (Seibert et al. 2000), in the past decades some authors derived diagnostic methods suitable for both moderate (San Jose and Casanova 1988; Joffre and Kangas 2001; Joffre et al. 2001) and free (Zilitinkevich 1972) convective conditions.

All the diagnostic equations assume at least a quasi-steady state. A typical scale for the convective turbulence is $\tau_* = h/w_*$ (Stull 1988), where w_* is the convective velocity scale, while a mixing-layer evolution time scale, associated with non-stationarity, can be defined

(Joffre et al. 2001) as $\tau_{ML} = h \, (dh/dt)^{-1}$. Taking typical values of h and w_* observed at Dome C, $\tau_* \approx 10^2$ s and $\tau_{ML} \approx 10^4$ s. Thus, the quasi-steady state assumption is generally fulfilled.

The relevant processes to consider for the convective ABL development and evolution are the exchange of heat between the land surface and the atmosphere, the background static stability, and the buoyancy effect, represented by the near-surface kinematic heat flux $\overline{(w'\theta')}_s$, the lapse rate γ, and the buoyancy parameter $\beta = g/T$, respectively. Other variables that could be included in the scaling analysis are u_* and f. As the dataset considered herein does not contain measurements at latitudes other than from Dome C, the dependence on f could not be investigated. However, as pointed out elsewhere (e.g. Joffre and Kangas 2001), the dependence on f appears to have only a secondary influence. In addition, as argued by Obukhov (1960), and later by Wyngaard and LeMone (1980), for convective conditions u_* is no longer an important similarity variable (as also shown in Sect. 3, Fig. 3b). For these reasons, in the estimate of h, u_* and f can be neglected.

To take into account the boundary-layer history, which can be represented using the cumulative heat input into the ABL, the instantaneous turbulent kinematic heat flux is substituted with a history scale defined by the time-averaged integral,

$$Q = \frac{1}{t_m - t_s} \int_{t_s}^{t_m} \left(\overline{w'\theta'}\right)_s dt,$$ (3)

where t_m is the time at which the measurement are taken, and t_s depends on the τ_{ML} value. Specifying t_d as the time at which $\overline{(w'\theta')}_s$ becomes positive, $t_s = t_d$ if $t_m - t_d \le \tau_{ML}$, and $t_s = t_m - \tau_{ML}$ if $t_m - t_d \ge \tau_{ML}$. Similar history scales were used by other authors to model different ABL parameters and characteristics, such as the height of the stable boundary layer (e.g. Stull 1983; Pournazeri et al. 2012), or the vertical structure of sea breezes (e.g. Steyn 2003). In the framework of the Buckingham Pi theorem, the selected parameters lead to a single non-dimensional group, that can be re-written as,

$$h = \alpha Q^{1/2} \gamma^{-3/4} \beta^{-1/4} = \alpha B,$$ (4)

where α is a coefficient to be determined experimentally, and B is the dimensional group

$$B = Q^{1/2} \gamma^{-3/4} \beta^{-1/4}.$$ (5)

Aside from the use of an integrated, rather than instantaneous, kinematic heat flux, Eq. 4 is consistent with the results reported previously. Zilitinkevich (1972) obtained a similar equation from dimensional analysis, but with a different relevant parameter, f instead of γ. Driedonks and Tennekes (1984) proposed a simple equation involving the buoyancy parameter, the turbulent heat flux, and a composite velocity scale that takes into account both w_* and u_*, but did not consider γ. More recently, Joffre et al. (2001) discussed and validated a diagnostic relation based on u_*/N (where N is the Brunt–Väisälä frequency), suitable for moderately unstable conditions only, and argued that the velocity scale should shift from u_* to w_* with increasing instability, leading to $h \propto w_*/N$. The latter can be rewritten as $h \propto \overline{(w'\theta')}_s^{1/2} \gamma^{-3/4} \beta^{-1/4}$, which is just Eq. 4 without the time-averaged integral.

As described in the previous section, the initial dataset was divided into two subsets. The first was used to retrieve α, the other to validate the proposed equation. For the lack of simplicity, the average τ_{ML} value observed at Dome C, $\tau_{ML} \cong 1.8 \times 10^4$ s (5 h), was used for all the days.

Figure 8a shows the dependence of the measured h on the values calculated by the dimensional group B for the retrieving dataset, and the related linear regression through the origin
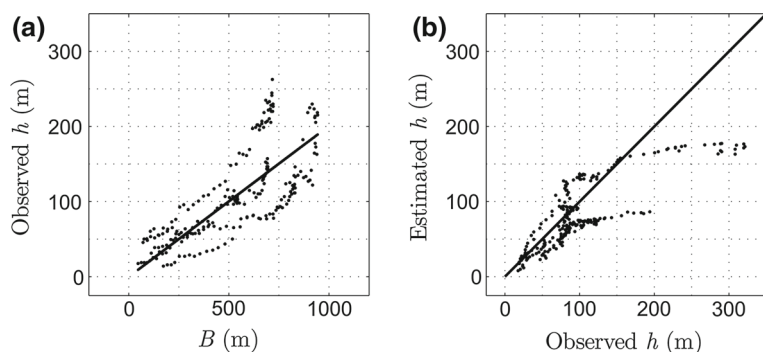
Fig. 8 Scatter plots of measured h against the dimensional group B (**a**) in Eq. 4, and against the h values (**b**) estimated by the same equation. The *full line* in panel (**a**) and (**b**) represents the linear fit through origin and the bisector, respectively

(continuous straight line). The coefficient $\alpha = 0.200 \pm 0.046$, and the retrieved value of the determination coefficient $R^2 = 0.89$, allow for a linear relationship between h and B. Figure 8b shows the scatter plot of measured against estimated h, obtained with Eq. 4 using the retrieving dataset, while Table 2 reports the model performance based on the statistical parameters listed in the previous section. The diagnostic model is in good agreement with the observed data ($IoA = 0.84$), although it tends to slightly underestimate the h values ($FB = 0.19$) at altitudes above approximately 100 m. As also shown in Fig. 7, all the statistical parameters considered in Table 2 indicate that the diagnostic model performance is comparable to that of the GBmodel with variable values of w_s.

5 Conclusions

Simultaneous measurements of the ABL mean and turbulent structure were performed at the French-Italian station of Concordia, on the Antarctic plateau, during the austral summer 2011–2012. Mixing-layer heights and turbulent fluxes were measured with high temporal and spatial resolution with a surface layer mini-sodar and a sonic anemometer, respectively. As in previous studies made at Concordia, in spite of the low surface temperatures a clear convective boundary-layer development was observed during the day, with heights ranging from about 25 up to 300 m.

The forecast h diurnal evolution obtained by the GBmodel with a fixed subsidence velocity provided an $IoA = 0.57$. Introducing the variation of the subsidence during the day, the GBmodel performance significantly increased ($IoA = 0.84$), and the underestimation of the observed h reduced of about 45 %. This improvement was particularly evident after midday, i.e. when the mixing-layer height remains almost constant, while the turbulent heat flux starts to decrease.

A diagnostic equation, based on dimensional analysis, was proposed and validated. The relevant parameters considered in the scaling analysis are the time-averaged integral of the kinematic heat flux, the background static stability, and the buoyancy effect. Despite its simplicity, the diagnostic model is in good agreement with the observed data ($IoA = 0.84$), and its performance is comparable to that of the more sophisticated GBmodel. Although the diagnostic models are applicable only under quasi-stationary condition, this result supports

the use of a limited number of variables to characterize the general convective mixing-layer behaviour.

References

Argentini S, Viola A, Sempreviva AM, Petenko I (2005) Summer boundary-layer height at the plateau site of Dome C. Antarctica. Boundary-Layer Meteorol 115(3):409–422

Argentini S, Pietroni I, Viola A, Zilitinkevich S (2007) Characteristics of the night and day time atmospheric boundary layer at Dome C, Antarctica. EAS Publ Ser 25:49–55

Argentini S, Mastrantonio G, Petenko I, Pietroni I, Viola A (2012a) Use of a high-resolution sodar to study surface-layer turbulence at night. Boundary-Layer Meteorol 143(1):177–188

Argentini S, Petenko I, Viola A, Mastrantonio G, Pietroni I, Casasanta G, Aristidi E, Genthon C, Conidi A (2012b) Thermal structure of the boundary layer over the snow: results from an under way experimental field at Concordia station, Dome C, Antarctica. In: 16th International symposium for the of boundary-layer remote sensing, Boulder, CO, 5–8 June 2012

Argentini S, Petenko I, Viola A, Mastrantonio G, Pietroni I, Casasanta G, Aristidi E, Genthon C (2013a) The surface layer observed by a high-resolution sodar at DOME C, Antarctica. Ann Geophys 56(5). doi:10. 4401/ag-6347

Argentini S, Pietroni I, Mastrantonio G, Viola AP, Dargaud G, Petenko I (2013b) Observations of near surface wind speed, temperature and radiative budget at Dome C, Antarctic Plateau during 2005. Antarct Sci, First View

Aubinet M, Vesala T, Papale D (2012) Eddy covariance, a practical guide to measurement and data analysis. Springer, Dordrecht, 270 pp

Batchvarova E, Gryning S-E (1990) Applied model for the growth of the daytime mixed layer. Boundary-Layer Meteorol 56:261–274

Batchvarova E, Gryning S-E (1994) An applied model for the height of the daytime mixed layer and the entrainment zone. Boundary-Layer Meteorol 71(3):311–323

Beyrich F (1993) On the use of SODAR data to estimate mixing height. Appl Phys B 57(1):27–35

Beyrich F (1997) Mixing height estimation from sodar data—a critical discussion. Atmos Environ 31(23):3941–3953

Beyrich F, Weill A (1993) Some aspects of determining the stable boundary layer depth from sodar data. Boundary-Layer Meteorol 63(1):97–116

Beyrich F, Weisensee U, Sprung D, Güsten H (1996) Comparative analysis of sodar and ozone profile measurements in a complex structured boundary layer and implications for mixing height estimation. Boundary-Layer Meteorol 81(1):1–9

Driedonks AG, Tennekes H (1984) Entrainment effect in the well-mixed atmospheric boundary layer. Boundary-Layer Meteorol 30:75–105

Faloona I, Mione J and Dumont M (2013) Measuring divergence and mean vertical velocities during the afternoon transition. In: BLLAST science meeting, Bergen, Norway, pp 14–16

Georgiadis T, Argentini S, Mastrantonio G, Viola A, Sozzi R, Nardino M (2002) Boundary layer convective-like activity at Dome Concordia, Antarctica. Nuovo Cimento C 25(4):425–431

Gryning S-E, Batchvarova E (1990) Analytical model for the growth of the coastal internal boundary layer during onshore flow. Q J R Meteorol Soc 116:187–203

Joffre S, Kangas M (2001) Simple diagnostic expressions for the stable and unstable atmospheric boundary layer height. WIT Trans Ecol Environ 47:67–74

Joffre SM, Kangas M, Heikinheimo M, Kitaigorodskii SA (2001) Variability of the stable and unstable atmospheric boundary-layer height and its scales over a boreal forest. Boundary-Layer Meteorol 99(3):429–450

King JC, Argentini SA, Anderson PS (2006) Contrasts between the summertime surface energy balance and boundary layer structure at Dome C and Halley stations, Antarctica. J Geophys Res 111(D2):D02105

Kossmann M, Vögtlin R, Corsmeier U, Vogel B, Fiedler F, Binder HJ, Kalthoff N, Beyrich F (1998) Aspects of the convective boundary layer structure over complex terrain. Atmos Environ 32(7):1323–1348

Lee X, Massman W, Law B (2004) Handbook of micrometeorology—a guide for surface flux measurement and analysis. Kluwer, Dordrecht, 250 pp

Mastrantonio G, Malvestuto V, Argentini S, Georgiadis T, Viola A (1999) Evidence of a convective boundary layer developing on the Antarctic Plateau during the summer. Meteorol Atmos Phys 71(1):127–132

Mastrantonio G, Viola A, Petenko I, Conidi A, Argentini S, Pietroni I (2010) Surface-layer mini-sodar for high-resolution studies of turbulent patterns. In: 15th International symposium for the advancement of boundary layer remote sensing, Paris, France, 28–30 June 2010

Myrup LO, Morgan DL, Boomer RL (1983) Summertime three-dimensional wind field above Sacramento. California. J Clim Appl Meteorol 22(2):256–265

Neff W, Helmig D, Grachev A, Davis D (2008) A study of boundary layer behavior associated with high NO concentrations at the South Pole using a minisodar, tethered balloon, and sonic anemometer. Atmos Environ 42(12):2762–2779

Obukhov AM (1960) On the structure of the temperature and velocity fields in the conditions of free convection. Izvestiya Akad Nauk SSSR 9:928–930

Ouwersloot HG, Vilà-Guerau de Arellano J (2012) Characterization of a boreal convective boundary layer and its impact on atmospheric chemistry during HUMPPA-COPEC-2010. Atmos Chem Phys 12(19):9335–9353

Pietroni I, Argentini S, Petenko I, Sozzi R (2012) Measurements and parametrizations of the atmospheric boundary-layer height at Dome C, Antarctica. Boundary-Layer Meteorol 143(1):189–206

Pournazeri S, Venkatram A, Princevac M, Tan S, Schulte N (2012) Estimating the height of the nocturnal urban boundary layer for dispersion applications. Atmos Environ 54:611–623

San Jose R, Casanova J (1988) An empirical method to evaluate the height of the convective boundary layer by using small mast measurements. Atmos Res 22(3):265–273

Seibert P, Beyrich F, Gryning SE, Joffre S, Rasmussen A, Tercier P (2000) Review and intercomparison of operational methods for the determination of the mixing height. Atmos Environ 34(7):1001–1027

Steyn DG (2003) Scaling the vertical structure of sea breezes revisited. Boundary-Layer Meteorol 107:177–188

Stull RB (1983) A heat-flux history length scale for the nocturnal boundary layer. Tellus 35A(3):219–230

Stull RB (1988) An introduction to boundary layer meteorology. Kluwer, Dordrecht, 666 pp

Van As D, Van den Broeke MR, Reijmer CH, Van de Wal R (2005) The summer surface energy balance of the high Antarctic plateau. Boundary-Layer Meteorol 115:289–317

Vickers D, Mahrt L (1997) Quality control and flux sampling problems for tower and aircraft data. J Atmos Ocean Technol 14:512–526

Wyngaard JC, LeMone MA (1980) Behavior of the refractive index structure parameter in the entraining convective boundary layer. J Atmos Sci 37(7):1573–1585

Zilitinkevich S (1972) On the determination of the height of the Ekman boundary layer. Boundary-Layer Meteorol 3(2):141–145